CHEMISTRY
A EUROPEAN JOURNAL

DOI: 10.1002/chem.200903125

Fatty Acid Carboxylate- and Anionic Surfactant-Controlled Delivery Systems That Use Mesoporous Silica Supports

Carmen Coll,[a, b] Elena Aznar,[a, b] Ramón Martínez-Máñez,*[a, b] M. Dolores Marcos,[a, b] Félix Sancenón,*[a, b] Juan Soto,[a] Pedro Amorós,[c] Joan Cano,[d, e] and Eliseo Ruiz[e]

Abstract: We report the preparation of a MCM-41 mesoporous material that contains the dye $[Ru(bipy)_3]Cl_2$ (bipy = bipyridine) inside the mesopores and functionalised with suitable binding groups at the entrance of the pores. Solids **S1**–**S3** were obtained by the reaction of the mesoporous material with *N*-methyl-*N*′-propyltrimethoxysilylimidazolium chloride, *N*-phenyl-*N*′-[3-(trimethoxysilyl)propyl]thiourea, or *N*-phenyl-*N*′-[3-(trimethoxysilyl)propyl]urea, respectively. A study of the dye delivery of these systems in buffered water (pH 7.0, 2-[4-(2-hydroxyethyl)piperazin-1-yl]ethanesulfonic acid (HEPES), 10^{-3} mol dm^{-3}) in the presence of a family of carboxylate ions was carried out. In the interaction of the anions with the surface of the solids, the response depends on the characteristics of the binding groups (i.e., imidazolium, urea and thiourea) at the pore outlets and their specific interaction with the corresponding anion. The interaction of long-chain carboxylate ions with the binding sites at the surface of the solids resulted in a remarkable inhibition of the delivery of the dye. This inhibition was observed clearly for the dodecanoate anion, whereas the octanoate, decanoate, cholate, deoxycholate, glycodeoxycholate and taurocholate anions induced a certain pore blockage that varied according to the solid studied. The interaction of smaller anions, such as acetate, butanoate, hexanoate and octanoate, with the solids had no effect on the dye release process. The possible use of the gating system for the chromo-fluorogenic detection of anionic surfactants through selective dye delivery inhibition was also explored. Molecular dynamic simulations that use force-field methods have been made to theoretically study the capping carboxylate mechanism. The calculations are in agreement with the experimental results, thus allowing a representation of the dye delivery inhibition in the presence of long-chain carboxylate ions.

Keywords: carboxylate ligands · controlled release · hybrid materials · mesoporous materials · molecular dynamics

[a] C. Coll, E. Aznar, Prof. R. Martínez-Máñez, Dr. M. D. Marcos, Dr. F. Sancenón, Dr. J. Soto
Instituto de Reconocimiento Molecular y Desarrollo Tecnológico
Centro Mixto, Departamento de Química
Universidad Politécnica de Valencia
Camino de Vera s/n. 46022, Valencia (Spain)
Fax: (+34) 96-387-93-49
E-mail: rmaez@qim.upv.es
fsanceno@upvnet.upv.es

[b] C. Coll, E. Aznar, Prof. R. Martínez-Máñez, Dr. M. D. Marcos, Dr. F. Sancenón
CIBER de Bioingeniería, Biomateriales y Nanomedicina (CIBER-BBN)

[c] P. Amorós
Institut de Ciència del Materials (ICMUV)
Universitat de Valencia
P.O. Box 2085, 46071 Valencia (Spain)

[d] Dr. J. Cano
Instituto de Ciencia Molecular (ICMol) and
Fundació General de la Universitat de València (FGUV)
Universitat de València, Paterna, Valencia, E-46980 (Spain)
Institució Catalana de Recerca i Estudis Avançats (ICREA)

[e] Dr. J. Cano, Dr. E. Ruiz
Departament de Química Inorgànica and
Institut de Química Teòrica I Computacional
Universitat de Barcelona, Diagonal 647, 08028 Barcelona (Spain)

Introduction

The combination of chemical principles and solid structures has recently resulted in the discovery of new synergic strategies, a unique tunability of the properties of nanoscopic solids and new perspectives of applicability to supramolecular concepts.[1] In this interdisciplinary area of "hetero-supramolecular" chemistry, one attractive concept is the development of the so-called molecular gating systems. A gating device can control mass transport and can ideally be "opened" and "closed" by certain target external stimuli (either chemical or physical). One appealing application of such systems is the design of functionalised nanocontainers with triggered structures for the development of advanced functional controlled release supports. Apart from the use of microcapsules,[2] micelles,[3] vesicles,[4] liposomes and so forth as nanocarriers, the use of silica mesoporous supports (SMPS) has recently attracted attention for use as systems in which gating functional scaffoldings could be coupled. The distinctive characteristics of mesoporous supports, such as high homogeneous porosity, easy surface functionalisation, inertness, stable structure, large surface area, biocompatibility and high load capacity, make these systems attractive scaffoldings for the development of systems for controlled delivery studies.[5]

The first example of gatelike structures in mesoporous materials was reported by Fujiwara et al., who used the reversible photodimerisation of coumarin to open/close the pores of a mesoporous scaffolding.[6] Since these reports, other photochemical gated systems, including the reversible light-driven *cis*/*trans* isomerisation of azobenzene groups,[7–9] association and light-operated dissociation of β-cyclodextrin with azobenzene groups,[10] and spiropyran/merocynine photoswitchable transformations,[11] have been reported.

The pH value has been another popular stimulus to control mass transport in mesoporous materials. We reported the first gated hybrid system to operate in aqueous solution controlled by modulation of the pH value and the presence of certain anions.[12,13] The gated material consisted of a mesoporous silica support functionalised with polyamines on the external surface. An approach that could be considered complementary was reported by Xiao and co-workers by using mesoporous surfaces functionalised with carboxylate ions.[14] Zink and co-workers reported the design, synthesis and functional behaviour of a pH-controlled supramolecular gatelike scaffolding that consisted of a [2]pseudorotaxane formation through the encirclement of dialkylammonium cations with the macrocyclic polyether dibenzo[24]crown-8,[15,16] by using ion–dipole interactions between curcubit[6]uril and bis-ammonium stalks[17] or by using the interaction between ferrocene derivatives and curcubit[7]uril.[18] Kim and co-workers demonstrated the controlled release of guest molecules by employing a pH-responsive gating ensemble that used mesoporous materials based on a cyclodextrin/polyamine pseudorotaxane motif.[19] Other more sophisticated dual controlled release systems have been developed. For example, we recently reported a gated hybrid system capped with boronic acid-functionalised gold nanoparticles that showed both a pH- and photo-switched release of guests.[20]

However, apart from light and pH-anions stimuli, perhaps the most popular approach to delivery control in mesoporous materials is the use of redox reactions. Lin and co-workers developed mesoporous functionalised materials for the controlled release of certain substances, such as drugs, DNA and so forth, by using mesoporous scaffoldings capped with CdS, gold, or magnetic nanoparticles.[21] The collaboration between Zink and Stoddart has also produced several examples of gated nanovalves triggered by redox inputs based on the use of rotaxanes and pseudorotaxanes that contain redox active stations, such as 1,5-dioxylnaphthalene and tetrathiafulvalene,[22–25] and Fujiwara et al. used a disilane–disulfide derivative to close the pores and opened them through the simple addition of dithiothreinol, which cleaves the disulfide bond.[26] Also, redox-induced release has been reported by Feng and co-workers by using mesoporous silica particles capped with a polymer network.[27]

Apart from the examples described above, which report the use of redox-, light- and pH-triggered systems, additional studies explore the use of other stimuli such as electrochemical oxidation,[18] temperature,[28] or enzyme-catalysed reactions.[29,30,31] In addition, we have also recently reported the capping of mesoporous materials with antibodies and selective gate opening in the presence of the corresponding antigen.[32] Most of these systems are designed for delivery applications, although we also consider that gating ensembles could possibly be used in the development of new signalling protocols, although little has been done so far in this direction.[33,34,35]

Despite these advances, the approach of gated smart supports for the development of real delivery scaffolds is still in the incipient stage. In particular, the possibility of designing the opening/closing of gated nanocontainers that could be controlled by chemical rather than physical stimuli is highly appealing and may open new perspectives of applicability to controlled release scaffoldings. Furthermore, it is apparent that few studies have been carried out on the development of gated mesoporous materials capable of varying delivery behaviour according to the anions present in the solution. With this objective in mind, we report herein the design of hybrid mesoporous materials that contain gatelike ensembles based on imidazolium, thiourea and urea binding groups, the solids being loaded with a suitable dye. The controlled delivery of the entrapped dye was studied in the presence of a family of carboxylic acids and surfactants in pure water. The possibility of using these systems in signalling protocols is also discussed. Part of this study has already been recently reported.[36]

Results and Discussion

Gated material: As stated above, the functionalisation of mesoporous scaffolds with certain gatelike ensembles has

proved a suitable procedure for the design of systems to study mass transport control (controlled delivery). In most cases, the designed systems consist of a switchable ensemble, able to respond to an external stimuli, anchored on a suitable nanocontainer and loaded with an entrapped substance to be delivered. For our study, we selected a mesoporous MCM-41 material that contains mesopores in the 2–3 nm range as the solid support. In relation to the molecular or supramolecular ensemble, we selected anion binding sites such as imidazolium, thiourea and urea derivatives. The delivery of a certain dye from the mesopores was studied in the presence of a family of carboxylate ions that can display a coordination interaction with the appended binding sites and eventually close the gate (Scheme 1).

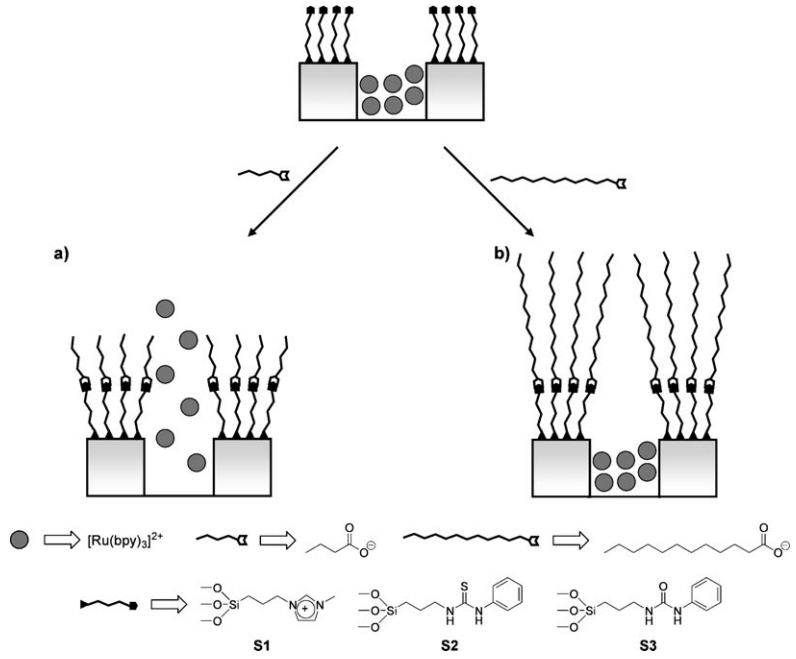

Scheme 1. A representation of the sensory hybrid materials and the interaction of the gatelike ensemble with a) butanoate (the gate remains "open") and b) dodecanoate anions (the gate is "closed")

For release protocols, the solid support must contain an entrapped guest (the dye) in the pores, whereas the molecular gating mechanism should ideally only be anchored on the outer surface (the pore outlets). The mesoporous MCM-41 support was synthesised with tetraethyl orthosilicate (TEOS) as a hydrolytic inorganic precursor and the surfactant hexadecyltrimethylammonium bromide (CTAB) as a porogen species. Calcination of the mesostructured phase produced the starting solid. The dye was added to a suspension containing the MCM-41 scaffolding, which was stirred for 24 h with the aim of completely loading the pores of the mesoporous support. The trimethoxysilyl derivatives *N*-methyl-*N*′-propyltrimethoxysilylimidazolium chloride, *N*-phenyl-*N*′-[3-(trimethoxysilyl)propyl]thiourea, or *N*-phenyl-*N*′-[3-(trimethoxysilyl)propyl]urea were added to this mixture to prepare the solids **S1**–**S3**, respectively. This reaction was carried out in the presence of a high concentration of the dye to disfavour the diffusion of the latter from the pores to the solution during grafting of the binding groups. By additionally taking into account that the reaction of the trimethoxysilyl derivatives with the silica surface is generally a quick process, it is feasible to deduce that the final structures will contain coordinating groups (i.e., imidazolium, urea or thiourea) anchored preferentially on the external surface and external entrance of the pore voids. A similar two-step synthetic procedure has recently been used both by us and others to develop responsive operational gating structures that contain a certain cargo in the pores and suitable switchable ensembles at the pore outlets. In all cases, the final solids were isolated by filtration and meticulously washed with different solvents and dried.

This procedure resulted in the preparation of solids that contain the anion binding groups imidazolium (**S1**), thiourea (**S2**) and urea (**S3**) anchored on the surface and a certain amount (see below) of dye entrapped in the mesopores. The imidazolium ion has been widely reported as a suitable coordination site for anions through electrostatic and $(C-H)^{+}\cdots X^{-}$ ionic hydrogen bonds.[37] On the other hand, the urea and thiourea moieties have also been used widely as anion-binding systems. It is known that these groups can act as double hydrogen-bond donors to give bidentate Y-shaped interactions with carboxylate ions.[38] These complexes have been reported to show appreciable stability, even in polar solvents.

Characterisation of the hybrid materials: Figure 1 shows powder X-ray diffraction (XRD) patterns of the as-synthesised MCM-41, calcined MCM-41 and the hybrid material **S1**. XRD studies of the as-synthesised MCM-41 shows four angle reflections typical of the hexagonal array that can be indexed as (100), (110), (200) and (210) Bragg peaks. A significant shift of the (100) reflection and broadening of the (100) and (200) peaks in the powder XRD study of the calcined MCM-41 sample is clearly appreciated in curve (b), thus corresponding to a cell contraction of approximately 6–8 Å due to the condensation of silanol during the calcinations step. Figure 1 also shows a curve that corresponds to **S1**. Reflections (110) and (200) are lost for this solid, most likely related to a decrease in contrast because of the filling of the pores with the ruthenium complex. Similar behaviour was observed for **S2** and **S3** (not shown). Nevertheless, the clear presence of the d_{100} peak in the XRD patterns suggests that the loading process with the $[Ru(bipy)_3]^{2+}$ complex and the additional function-

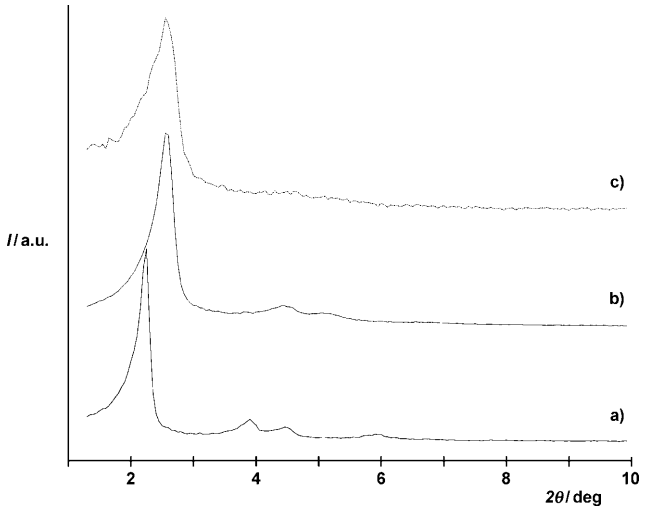

Figure 1. Powder X-ray patterns of the a) as-synthesised MCM-41, b) calcined MCM-41 and c) the final solid **S1** that contains the dye and the anchored imidazolium derivatives.

alisation with the imidazolium, thiourea and urea derivatives did not substantially modify the mesoporous MCM-41 support. The presence of the mesoporous structure in the funcionalised solids is also confirmed by TEM analysis, in which the typical hexagonal porosity of the MCM-41 matrix can clearly be observed (Figure 2).

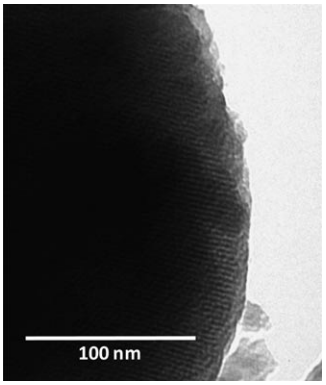

Figure 2. TEM image of **S1** that shows the typical porosity of the MCM-41 matrix.

After functionalisation, the IR spectra of **S1**–**S3** show the expected features, namely, intense bands due to the silica matrix ($\tilde{\nu}=1250$, 1087, 802, 462 cm^{-1}) and vibrations of water molecules ($\tilde{\nu}=3420$, 1620 cm^{-1}). As the funcionalisation of the solids is low, it is not possible to observe the characteristic bands of the anchored organic moieties. However, a drop in intensity of the band at $\tilde{\nu}=952$ cm^{-1} related to the vibration of the silanol group was observed, thus indicating surface functionalisation.

Quantification of the content of the binding group and the $[Ru(bipy)_3]^{2+}$ dye was accomplished by thermogravimetric analysis (TGA) and elemental analysis. The typical content of the dye and imidazolium, thiourea and urea groups in the final solids **S1**–**S3** are shown in Table 1.

Table 1. Amount of the imidazolium, thiourea and urea groups and dye present in the **S1**–**S3** sensory materials.

Solid	Binding groups [wt%]	Dye [wt%]
S1	9	10
S2	7	19
S3	5	15

The solids were also characterised by UV/Vis spectroscopic measurements. The UV/Vis diffuse reflectance spectrum of **S2** shows an intense absorption band at $\lambda=470$ nm that corresponds to the $[Ru(bipy)_3]^{2+}$ complex inside the pores (Figure 3). Similar spectra were obtained for **S1** and **S3** (data not shown).

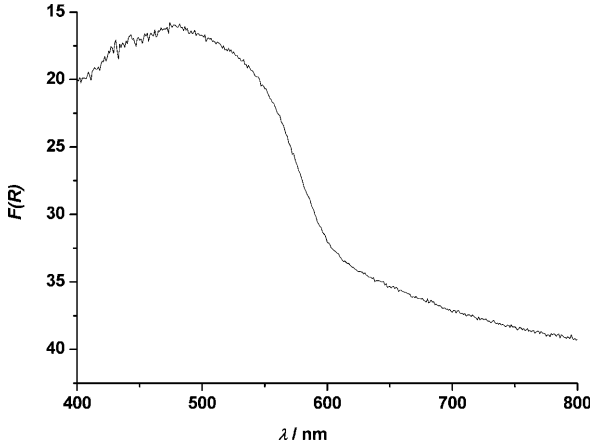

Figure 3. Diffuse reflectance UV/Vis spectra of **S2**.

The nitrogen adsorption–desorption isotherms of the calcined MCM-41 material shows a typical curve for these mesoporous solids; that is, an adsorption step at intermediate value (0.3). This curve corresponds to a type IV isotherm, in which the observed step can be related to nitrogen condensation inside the mesopores by capillarity. The absence of a hysteresis loop in this interval and the narrow pore distribution suggests the existence of uniform cylindrical mesopores (0.90 $cm^3 g^{-1}$). Application of the BET model[39] gave a value for the total specific surface of 1371.6 $m^2 g^{-1}$. From XRD studies, porosity and TEM studies, the cell parameter a_o, pore diameter and wall thickness (39.97, 23.2 and 16.76 Å, respectively) can be calculated. The volume and pore size were estimated by using the Barret–Joiner–Haselda (BJH) method.[40] The isothermal nitrogen adsorption/desorption behaviour of **S1**–**S3** were also studied (Figure 4). In contrast to the MCM-41 starting materials, **S1**–**S3** show almost flat curves, thus indicating a remarkable decrease of porosity (Table 2). This result could be expected, bearing in mind the high content of the $[Ru(bipy)_3]^{2+}$ complex that fills the

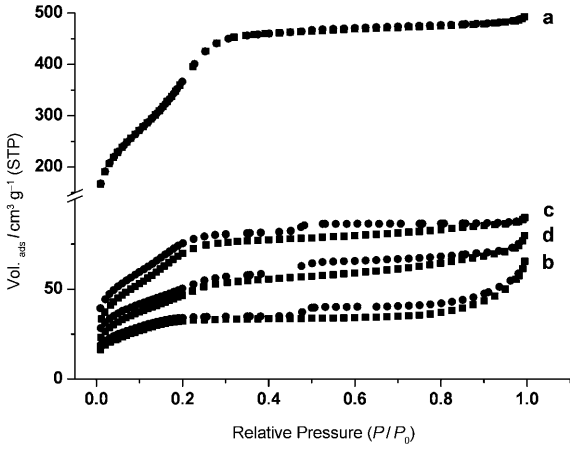

Figure 4. Nitrogen adsorption/desorption isotherms for a) the mesoporous MCM-41 material, b) **S1**, c) **S2** and d) **S3**.

Table 2. BET specific surface values, pore volume and pore size calculated from the nitrogen adsorption/desorption isotherms for **S1**–**S3**.

Sample	S_{BET} [$m^2 g^{-1}$]	BJH pore[a] [nm]	Total pore volume[b] [$cm^{-3} g^{-1}$]
MCM-41	1371	2.3	0.91
S1	122	2.0	0.08
S2	266	2.1	0.19
S3	172	2.2	0.12

[a] Pore estimated by using the BJH model applied on the adsorption branch of the isotherm. [b] Total pore volume according to the BJH model.

pores. We had previously observed similar behaviour in other gated materials. Therefore, the total lack of porosity provides direct evidence of the high efficiency of the dye loading.

Delivery in the presence of carboxylate ions: A study was made of the effect of certain anions on the control of the dye delivery. In the first step, the capacity of **S1**–**S3** to deliver the ruthenium(II) dye in the presence of different carboxylate ions ($CH_3(CH_2)_nCOO^-$; $n=0$, 2, 4, 6, 8, 10) was tested in aqueous solution. The longer carboxylate ions ($n>10$) were poorly soluble in water and were not studied. In the preliminary scanning, the response of the solids in the presence of carboxylate ions was very similar in the range pH 5–8. Lower pH values were not studied because of the lower solubility of the protonated carboxylic form, whereas higher pH values were avoided because of possible attack by the OH^- ion on the silica matrix. A neutral pH value was finally selected for the study (pH 7.0, 2-[4-(2-hydroxyethyl)piperazin-1-yl]ethanesulfonic acid (HEPES), 10^{-3} mol dm^{-3}). In a typical release experiment, the solid (10 mg) was suspended in water (25 mL) that contained the corresponding carboxylate ion ($c_{carboxylate}=10^{-3}$ mol dm^{-3}). The suspension was stirred until complete diffusion of the $[Ru(bipy)_3]^{2+}$ complex from the pore voids into the bulk solution was observed. Maximum delivery was detected after approximately 30 minutes (see below). Finally, the mixture was filtered. The delivery of the dye was directly monitored through the spin-allowed metal-to-ligand change-transfer (MLCT) transition band of the $[Ru(bipy)_3]^{2+}$ dye centred at $\lambda=454$ nm in the aqueous phase.

The delivery of the dye from the pore voids for **S1**–**S3** in the presence of carboxylate ions is shown in Figure 5, which plots the difference in absorbance at $\lambda=454$ nm for the dye delivered from the solid and for the corresponding solid/carboxylate ion system. Values near zero indicate that there was no pore blockage, whereas higher values mean that dye delivery was inhibited.

The chromogenic response is most likely related to the ability of the positively charged imidazolium ion and the neutral thiourea and urea moieties to form complexes with carboxylate ions. The small carboxylate ions do not have any effect, whereas the longer ions induce partial or total delivery inhibition (Figure 5). Solids **S2** and, especially, **S3** show a gradual increase in release inhibition as the length of the carboxylate ion increases. In contrast, there is no gradual pore blockage for **S1**, but rather an "on/off" behaviour; that is, complete dye delivery for small carboxylate ions (from acetate to octanoate), which can not "close" the gate and complete blockage for longer carboxylate ions, which act as molecular taps in the gatelike ensemble. Coordination of a small or medium carboxylate ion, such as octanoate or smaller, does not inhibit dye release from the pores to the bulk solution. On the other hand, on coordination with the imidazolium ion, the dodecanoate ion would form a highly hydrophobic layer around the entrance to the pores that would inhibit the delivery of the otherwise rather hydrophilic ruthenium(II) dye from inside the pores to the water phase. The small differences in the behaviour of **S1**–**S3** in the presence of carboxylate ions are modulated and are likely due to the differences in the nature of the binding sites.

The release kinetics at neutral pH was studied in more detail for **S1** and two carboxylate ions ($c_{carboxylate}=10^{-3}$ mol dm^{-3}), for which a clearly different behaviour was observed; that is, the octanoate and dodecanoate ions, for which a remarkably different dye delivery process is seen (Figure 6). It also can be observed that maximum dye liberation is found after approximately 30–40 minutes. A similar kinetic release (not shown) to that of the octanoate ion was found for only **S1** in the presence of shorter carboxylate ions, such as acetate, butanoate and hexanoate.

The different behaviour displayed by the octanoate versus dodecanoate ion can also be seen in Figure 7, which shows adsorption versus $-\log c_{carboxylate}$ curves for these carboxylate ions with **S1** in water. The dodecanoate ion can completely inhibit dye delivery from **S1** at the millimolar level, whereas the octanoate ion does not have any effect on delivery, even at very high concentrations of up to 10^{-2} M.

An interesting question related to this system is the evaluation of the imidazolium/carboxylate ion interaction. It is evident from Figure 6 that whereas the dodecanoate ion can inhibit the delivery of the dye, the octanoate ion can not display the same behaviour. This outcome may be related to

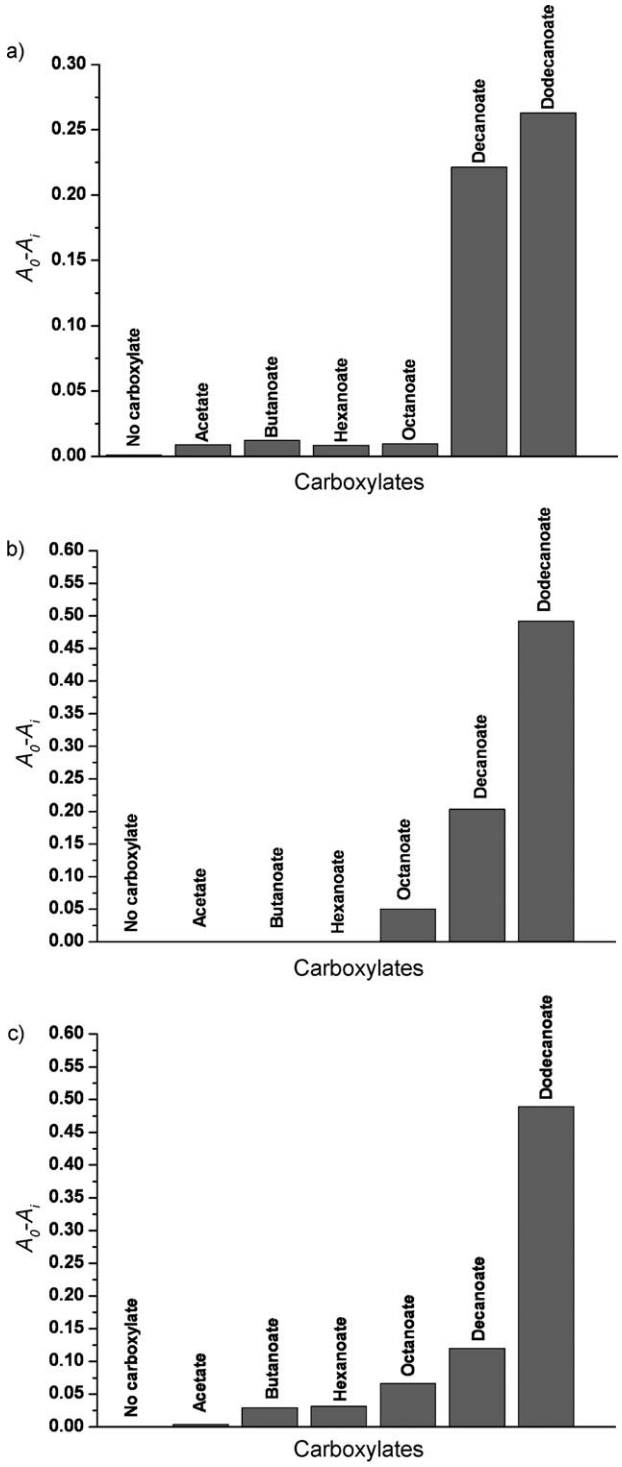

Figure 5. Colorimetric response of a) **S1**, b) **S2** and c) **S3** materials in the presence of carboxylate ions of different length at neutral pH in water. The difference in the absorbance for the solid system alone A_0 and the absorbance for the corresponding solid/carboxylate ion system A_1 is shown. $t=1$ h

the possibility that the dodecanoate ion can interact with the imidazolium ions and that this interaction may not be possible for the octanoate ion. Additional experiments were carried out to rule out this possibility. When an excess of a

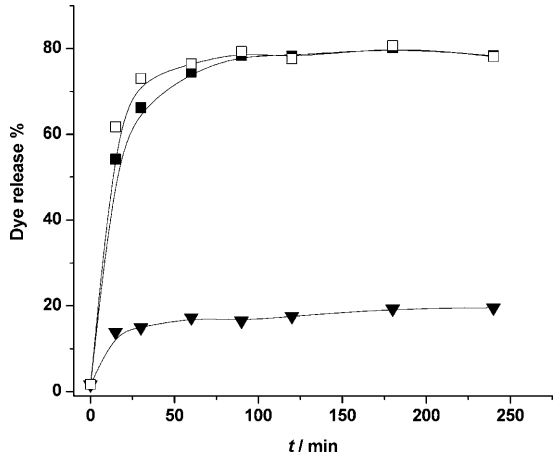

Figure 6. Colorimetric dye release kinetics for **S1** in water (pH 7.0, HEPES, 10^{-3} mol dm^{-3}) in the presence of octanoate (■) or dodecanoate (▼) ions ($c_{\text{carboxylate}}=10^{-3}$ mol dm^{-3}) and without carboxylate ions (□).

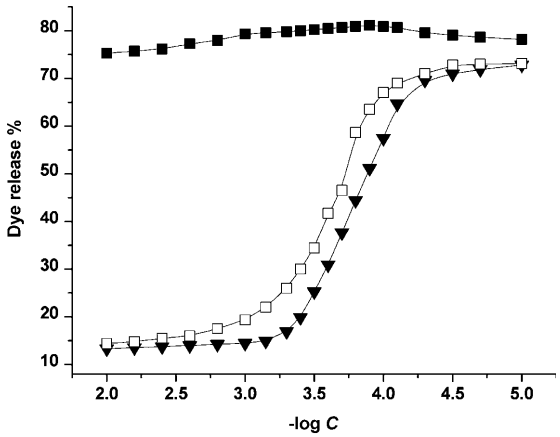

Figure 7. Variation in the absorption ($\lambda=454$ nm) versus the logarithm of the concentration for dodecanoate (▼) , decanoate (□) and octanoate (■) ions with the sensory material **S1** in water. $t=1$ h.

certain carboxylate ion is added to **S1**, the TGA and elemental analysis clearly show an increase in organic material, thus indicating that self-assembly of the corresponding carboxylate ion occurs on the imidazolium surface. However, it turned out to be rather difficult to obtain reliable quantitative results of the anchored carboxylate ion through interaction with the imidazolium ion from TGA and elemental analysis. As the possible cause of error, we suggest the presence of the $[Ru(bipy)_3]^{2+}$ dye at the pores, which is partially delivered even in short reaction times in the presence of the carboxylate ions. Moreover, for MCM41-type solids, below 300 °C water loss is typically observed due to the condensation of an undetermined number of silanol groups, thus making quantitative interpretation rather complex. Due to this reason, we opted to use a simpler solid support to carry out studies on the imidazolium/carboxylate ion interactions. Thus, a simple fumed-silica support was prepared (similar to the MCM-41 material with no mesopores or the dye) and functionalised with the imidazolium binding sites to make

suitable assays. This material was readily obtained by reaction of the *N*-methyl-*N*′-propyltrimethoxysilylimidazolium chloride derivative in fumed silica in acetonitrile at room temperature to produce solid **FS-Im**, which was characterised by using conventional solid-state techniques. The imidazolium content was determined by TGA and elemental analysis. The molar ratio between the imidazolium binding molecule and SiO_2 was 5.3×10^{-2} (0.67 mmol per g solid), which provides a relatively dense monolayer of imidazolium cations with an average distance between neighbouring imidazolium ions of approximately 10 Å. We used this **FS-Im** support to study the interaction with two different guests, that is, octanoate and dodecanoate ions. For this purpose, aqueous suspensions of **FS-Im** were titrated with these two carboxylate ions and the titrations were followed by conductimetry. Figure 8 shows the conductivity of the solution as a function of the number of equivalents of carboxylate ion added (equivalents with respect to the equivalents of imizadolium ions in the solid; i.e., 0.67 mmol per g solid).

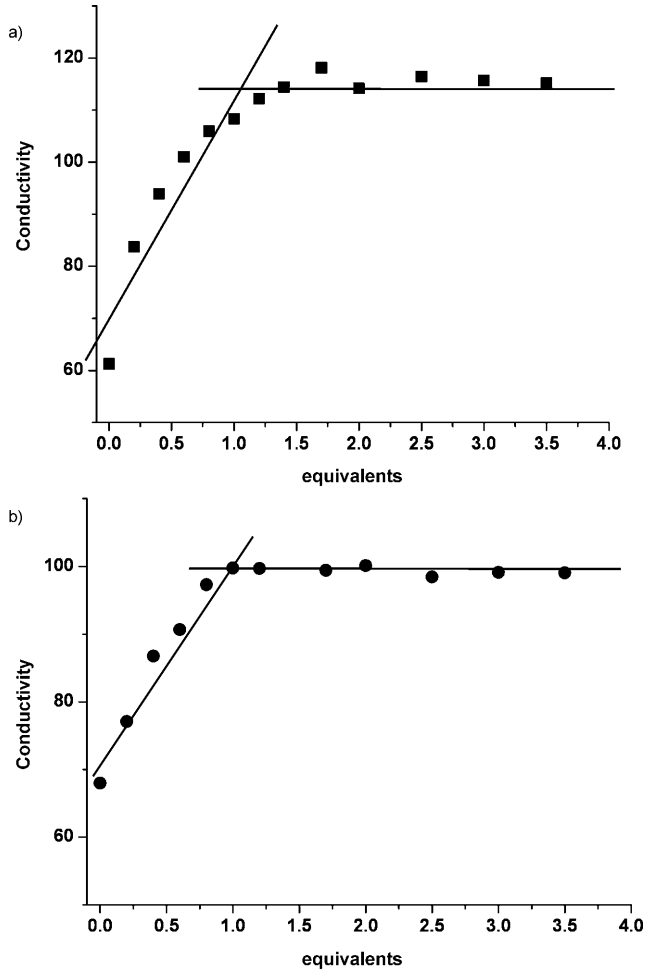

Figure 8. Conductivity versus the number of equivalents of carboxylate ions added in the titration experiments of solid **FS-Im** with a) octanoate and b) dodecanoate ions. The difference in the conductivity of an aqueous suspension of **FS-Im** in the presence of a certain amount of carboxylate ion and an aqueous solution that contains the same quantity of carboxylate ion is shown.

From these titration profiles, it can be seen that a significant change in conductivity is observed for both carboxylate ions at one equivalent of added carboxylate ion. The results undoubtedly show that for both the octanoate and dodecanoate ions a monolayer of carboxylate ions is formed coordinated to the imidazolium-functionalised surface. By extrapolating this result to **S1**, it seems clear that both carboxylate ions coordinate on the imidazolium surface at the pore boundaries and in both cases the substitution of a chloride group by the corresponding carboxylate ion would surely be complete, as with **FS-Im**. This behaviour means that the difference observed between the dodecanoate and octanoate ions (Figures 6 and 7) is not only due to different densities of the **S1**/carboxylate ion at the pore outlets, depending on the carboxylate used, but is most likely due to the "gatelike" effect.

Finally, we were particularly concerned with the possibility that the observed behaviour was caused by a simple interaction of the carboxylate ion with the silica surface. To rule out this possibility, the delivery experiments were repeated using a MCM-41 support loaded with the dye but not functionalised with the imidazolium ion. This solid shows no selectivity and has similar dye release kinetics for all the carboxylate ions. Therefore, it can be concluded that the colorimetric sensing discrimination observable to the naked eye of the long-chain carboxylate ions only occurs in solids that contain both nanoscopic pores and a coordinating group at the entrance to the pores.

We were also interested in studying the behaviour of these solids in the presence of other anions and found in preliminary studies that the interaction of **S1**–**S3** with the cholate, doexycholate, glycodeoxycholate and taurocholate anions resulted in a partial pore blockage. These ions are the corresponding anions of primary bile acids and play a fundamental role in the metabolism of cholesterol.[41] Further assays were carried following experimental procedures similar to that described above with the corresponding solid (10 mg) in water at neutral pH. Capping of the solids in the presence of the cholate, deoxycholate, glycodeoxycholate and taurocholate ions was evaluated by monitoring the visible absorption band when the dye was released into the solution. The results for **S2** and **S3** are shown in Figure 9, which also includes the response of this solid to the dodecanoate ion for comparative purposes. The capping ability of the anions tested on **S2** is on the order dodecanoate ~ deoxycholate ~ glycodeoxycholate > cholate > taurocholate and a similar trend was observed for **S3** and **S1** (not shown). Of the anions tested, the taurocholate ion shows the lowest capping ability, most likely due to the weaker interaction of the sulfonate unit of the taurocholate anion with the binding sites on the solids relative to the analogous carboxylate ions. It is also interesting to note that small differences in the structure of the anions and the anchored binding groups on the solids give slightly different final responses. To sum up, the studies carried out with **S1**–**S3** demonstrated that a family of carboxylate ions can modulate the delivery of the entrapped guest through interaction with the binding groups

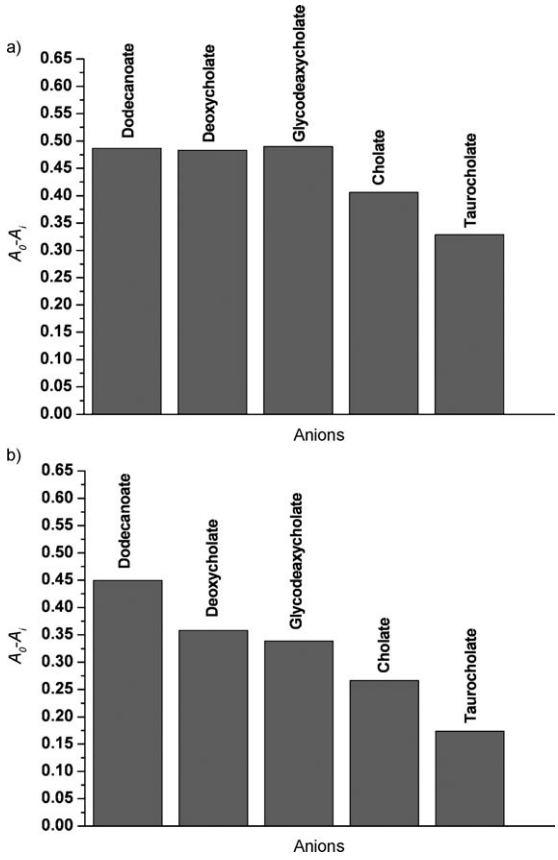

Figure 9. Colorimetric response of a) **S2** and b) **S3** in the presence of the cholate, deoxycholate, glycodeoxycholate and taurocholate ions at neutral pH in water. The difference in absorbance for the solid system alone A_0 and the absorbance for the corresponding solid/carboxylate system A_1 is shown. For comparative purposes, the dye delivery from the solids in response to the dodecanoate ion is also included. $t=1$ h.

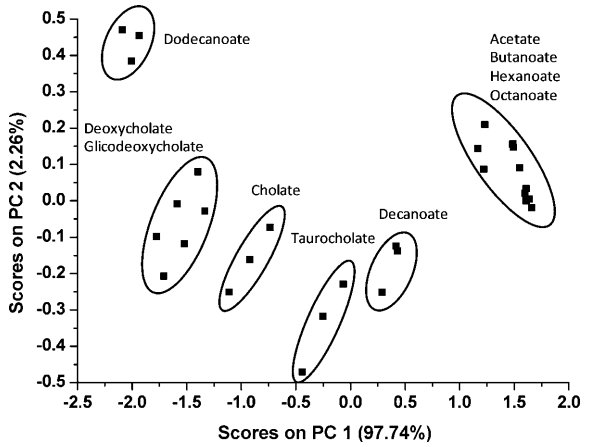

Figure 10. PCA score plot for the acetate, butanoate, hexanoate, octanoate, decanoate, dodecanoate, cholate, deoxycholate, glycodeoxycholate and taurocholate ions with **S1**–**S3** (the data shown are from three different trials). The PC axes are calculated to lie along lines of diminishing levels of variance in the data set.

anchored on the external surface of the mesoporous material. In addition, the degree of capping of the anions studied depends on the characteristics of both the anion and binding groups. Therefore, the response of a certain solid in the presence of a certain anion depends on the intrinsic chemical nature of the binding site, shape and size of the anion, possibility of densely packed monolayers and so forth. These subtle differences are reflected in the specific final delivery behaviour of each solid–anion ensemble.

To study the different response of the solids with different anions, the responses of **S1**–**S3** could be combined to form ensembles for the pattern recognition of anions in an attempt to find selectivity fingerprints. This approach can be carried out, for example, when the data matrix is analysed by principal component analysis (PCA) algorithms.[42] The PCA score plot of the results for **S1**–**S3** in the presence of the anions studied over three different trials is shown in Figure 10. Recognition patterns can be identified clearly for some of the anions studied. A detailed look at the PCA plot suggests that there is some correlation between the position of the anion clusters on the PC1 axis and their size. Thus, HEPES (no anion) and the carboxylate ions acetate, butanoate, hexanoate and octanoate appear together in the same zone at positive values of PC1. The low discrimination is in agreement with the very similar response found for all these species (no pore blockage). The remaining anions are placed at medium and negative values of PC1. A clear differentiation between the clusters for the decanoate and dodecanoate ions is observed. Also, different overall behaviour was found for the cholate and taurocholate ions, whereas the deoxycholate and glycodeoxycholate ions form a unique cluster in the PCA space.

Signalling applications—sensing of anionic surfactants: One suggested application for stimuli/responsive systems is their use as triggered structures for the development of advanced functional controlled release supports. These materials are promising, for example, in the design of functional tailor-made nanodevices for on-command drug/gene/protein delivery, self-healing and so forth. From a different point of view, we have also suggested that these materials can be used for signalling applications.[33–35] In our case, the hybrid material has been loaded with a dye and the system is designed to be uncapped. The addition of the solid to a solution that contains the target analyte results in capping of the pores and inhibition of the dye delivery. With regard to closing the pores as a consequence of the selective interaction with the gatelike binding sites (as in our case, for example, the interaction of the large carboxylate ions with the binding site groups), the recognition process becomes a selective optical response. This remarkable colorimetric "on/off" discrimination of long-chain carboxylate ions in water is, as far as we know, difficult to achieve by using conventional molecular probes. In fact, colorimetric sensors for long-chain carboxylate ions are scarce and many of these probes show nonspecific chromo-fluorogenic responses to the carboxylate functional ion. There are also few examples of the colorimetric discrimination of individual members or subgroups of carboxylate families in organic solvents[43] or water.[44]

After the detailed study of the interaction of imidazolium, urea, or thiourea moieties with different carboxylate ions and the effect of this interaction on the delivery of the dye from the mesoporous scaffoldings, we further explored the possible use of the gating system for the selective chromo-fluorogenic detection of anionic surfactants. It was envisioned that the very same inhibition effect observed in the presence of the dodecanoate ion with **S1**, which contained imidazolium ions, would be operative in the presence of anionic surfactants, which also contain an anionic groups and a hydrophobic tail. We have previously demonstrated that anionic surfactants have an affinity for forming complexes with imidazolium-functionalised surfaces.[45] Accordingly, we considered that the interaction between an imidazolium derivative and an anionic surfactant could be conveniently applied to the colorimetric determination of these environmentally important anions through dye delivery inhibition in functionalised nanoporous solids such as **S1**. At this point, it might be worth commenting that the easy detection of anionic surfactants in water is still an unresolved goal. For example, many commonly reported methods require time-consuming procedures (e.g., titrimetry,[46] chromatography[47]), need time-consuming sample preparation (e.g., spectrophotometry,[48] spectrofluorimetry[49]), use large amounts of harmful solvents (e.g., CH_3Cl in the standard well-known spectrophotometric "methylene blue" method), or show problems related to reproducibility and signal stability (typically found in ion-selective electrodes).[50] In addition, many of these methods are also not generally suitable for quantitative or semiquantitative assays in situ.

Lauryl sulfate (LS^-) and dodecylphosphate (DP^-) were selected as anionic surfactants and **S1** was chosen as the sensing solid for these studies. Analysis of the response was tested simply by using **S1** (10 mg) suspended in water (25 mL; pH 7.0, HEPES, 10^{-3} mol dm^{-3}) that contained the corresponding anion ($c_{anion} = 10^{-3}$ mol dm^{-3}) and stirring the suspension for 30 minutes. For the sake of comparison, the response was also studied in the presence of the cationic cetyltrimethylammonium (CTA^+) and the zwitterionic Triton X-100 surfactants and compulsory water-present anions and cations, such as Na^+, K^+, Ca^{2+}, CO_3^{2-}, PO_4^{3-} and SO_4^{2-}. The colorimetric response of **S1** to these species is shown in Figure 10, which plots the absorbance difference at $\lambda =$ 454 nm for the dye delivered from **S1** and the corresponding solid/anionic surfactant system. The anionic surfactants LS^- and DP^- show a quite similar capping ability relative to the dodecanoate ion, whereas the cationic and zwitterionic surfactants can not inhibit the dye release. Also, except for some response to phosphate, **S1** shows a poor response to inorganic cations and anions. Figure 10 suggests that **S1** or similar systems could be used for the development of screening probes for the colorimetric detection of anionic surfactants in water through dye delivery inhibition by using mesoporous ensembles containing binding sites on the pore outlets. Further analytically oriented studies are being carried out in our laboratory. We carried out a competitive experiment with **S1** to study the possibility of using these systems for the selective chromo-fluorogenic detection of anionic surfactants in real samples. In this respect, **S1** (10 mg) was suspended in water (25 mL; pH 7.0, HEPES, 10^{-3} mol dm^{-3}) containing phosphate, nitrate, acetate, butanoate and LS^- ions ($c_{anion} = 10^{-3}$ mol dm^{-3}). The colorimetric response of **S1** under these conditions is shown in Figure 11. The dye release inhibition in a mixture containing LS^- and the interferents is nearly the same relative to LS^- alone.

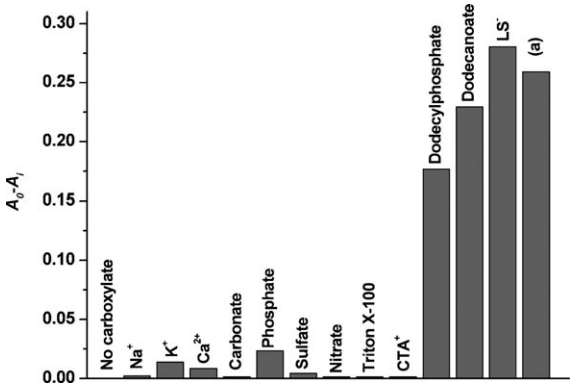

Figure 11. Colorimetric response of **S1** in the presence of anionic (LS^-, DP^-), cationic (CTA^+) and neutral (Triton X-100) surfactants and inorganic cations and anions ($c = 10^{-3}$ mol dm^{-3}). The difference in absorbance for the solid system alone A_0 and the absorbance for the corresponding **S1**–anion/cation system A_I is shown. $t = 1$ h. a) A mixture containing phosphate, nitrate, acetate, butanoate and LS^- ions ($c_{anions} = 10^{-3}$ mol dm^{-3}).

Computational studies: As we have discussed above, capping of the pores is most likely related to the interaction of long-chain carboxylate ions with the anchored binding groups on the surface of the mesoporous solids. In addition, to study this interaction in further detail, the carboxylate-controlled modulation of the gate ensemble was studied by molecular dynamic simulations with force-field methods by selecting the solid functionalised with imidazolium ions. With this goal, a mesoporous silica structure was constructed by taking the plane (1−11) of the β-cristobalite structure as a base on which large hexagonal nanopores were included (see the Experimental Section). This model shows a hexagonal supercell with the following parameters: $a = b =$ 40.503 Å, $\alpha = \beta = 90.0°$ and $\gamma = 120.0°$. The size of this "supercell" was chosen to generate pores and walls with similar dimensions ($d = 22.9$, $t = 15.5$ Å) to those dimensions experimentally found in the prepared MCM-41-based solids ($d =$ 23.3, $t = 13.1$ Å). The corresponding imidazolium derivatives were anchored on this scaffolding to the external surface. Because of the difficulty in finding the global energy minimum, molecular dynamic simulations were performed to cover the most important parts of the potential-energy surface by using thermal energy to escape from local minima (see the Experimental Section). The starting system was built by placing the carboxylate molecules on the nanopore of the mesoporous surface. Dynamic simulations and subsequent geometry optimisation on the model showed that the

carboxylate ion moved in proximity to the imidazolium ions influenced by electrostatic interactions. At the starting point, two models were tested in which the carboxylate molecules were placed so that the carboxylic or alkyl portions of the molecule pointed towards the pore (Figure 12a,b),

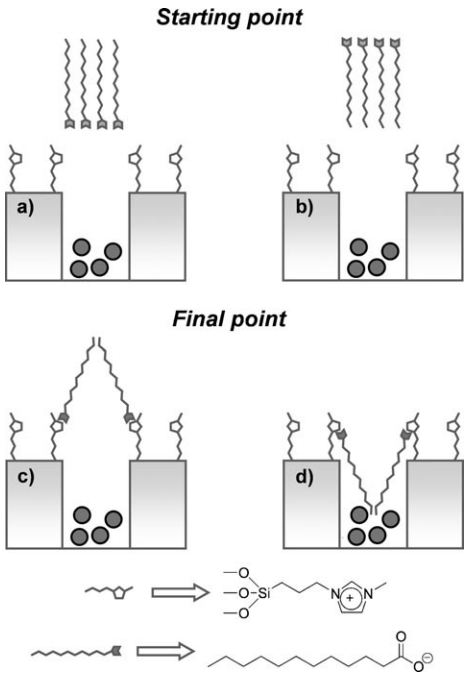

Figure 12. Starting points of the two models tested (see text) at which the carboxylate ions were placed pointing towards the pore with the a) carboxylic or b) alkylic portions of the molecule and the possible final interactions (c,d).

thus expecting that the final conformation may be different depending on the initial situation of the carboxylate ions (Figure 12c,d). However, it was observed that the studied carboxylate ions moved in all cases to final positions similar to those shown in Figure 12c in which the attached imidazolium rings interact with the carboxylate ions that are situated in the outer part of the mesopores. Although not the central issue of this study, it is also noteworthy that geometry optimisation carried out on surfaces not completely covered by imidazolium ions suggested a strong interaction of the carboxylate ions with the positive charge on the silicon atoms. In fact natural-bond-orbital (NBO) analysis carried out on the B3LYP wave function showed that the charge presented by the silicon atoms at the surface is larger than the charge observed on the imidazolium ring, which delocalises the charge over the rest of ligand. Thus, the nitrogen atoms in the ring have a negative charge and the positive charge on the ring is mainly placed on the hydrogen atoms.

When dynamic simulations and subsequent geometry optimisation on the interaction of imidazolium ions on the surface was carried out for a family carboxylate ions (CH_3-$(CH_2)_nCOO^-$; $n=0$, 2, 4, 6, 8, 10), it was clearly observed that the nanopore diameter decreased as a function of the length of the carboxylate ion (for example, Figure 13 shows a parallel perspective views of the surfaces of the models with the acetate and decanoate anions). The change in the

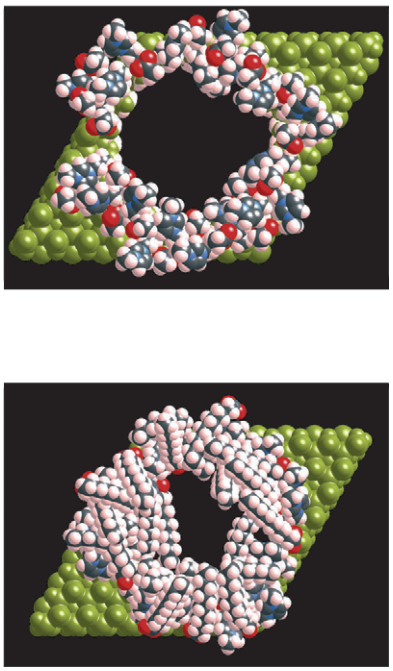

Figure 13. Parallel perspective views of the surfaces of models with a) acetate and b) decanoate. Pale yellow, blue, grey, red and pink have been employed for the mesoporous base, nitrogen, carbon, oxygen and hydrogen atoms, respectively.

size of the nanopore (d; calculated with the simulation model) with the length of the alkyl chain of the carboxylate ion is displayed in Figure 14. In addition, an estimation of the molecular diameter for the $[Ru(bipy)_3]^{2+}$ complex ($d_{Ru} \approx 12$ Å) can be calculated from the Van der Waals radii by supposing a spherical geometry for this complex. Moreover, it has to be taken into account that the model is a dynamic system in which the pore diameter continuously changes,

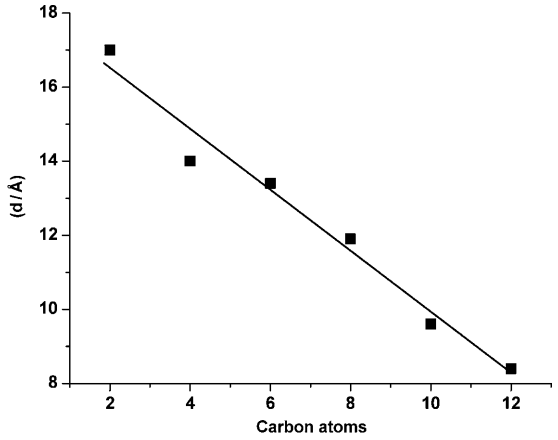

Figure 14. Dependence of the nanopore diameter d [Å] as a function of the number of carbon atoms in the $CH_3(CH_2)_nCOO^-$ ions.

but with averaged values that are close those calculated values. Thus, the theoretical results must be considered only in a qualitative way. Nevertheless, it can be concluded from a comparison between the values of the d and d_{Ru} parameters that the ruthenium complex can be released for alkyl carboxylate ions with carbon atoms of ≤ 8 (octanoate), which is in agreement with the experimental observation. In summary, the model shows that carboxylate ions that interact with imidazolium ions at the pore outlets can significantly decrease the pore diameter, thus eventually resulting in pore blockage and dye release inhibition, which is in agreement with the experimental observations when using long-chain carboxylate ions.

Conclusion

The development of suitable mass-control systems is a promising area of research with a wide range of applications from complex controlled delivery systems to novel sensing paradigms. A study was carried out on the delivery of the dye $[Ru(bipy)_3]^{2+}$ from mesoporous materials that contained anion binding sites, such as imidazolium, thiourea and urea, on the pore outlets in the presence of certain anions. Large-scale dye delivery was obtained in the presence of small carboxylate ions (from acetate to octanoate) that could not "close" the gate, whereas complete blockage was observed for longer carboxylate ions, which act as molecular taps in the gatelike ensemble. For longer carboxylate ions, the delivery inhibition effect is attributed to the formation, on coordination with the binding groups, of a highly hydrophobic layer around the entrance to the pores that inhibits the delivery of the otherwise rather hydrophilic ruthenium(II) dye from inside the pores to the water phase. Small differences in the behaviour of **S1**–**S3** in the presence of the carboxylate ions are modulated, probably due to the differences in the nature of the binding sites. The partial delivery of the dye from the functionalised solids was also observed in the presence of the bile anions cholate, deoxycholate, glycodeoxycholate and taurocholate. A possible use of the gating system for the chromo-fluorogenic detection of anionic surfactants was also explored. A selective dye delivery inhibition from **S1** in water was observed in the presence of the anionic surfactants lauryl sulphate and dodecylphosphate, whereas no response was found for the cationic CTA^+ and zwitterionic Triton X-100 surfactants. Finally, the experimental carboxylate control of mass transport has also been studied by means of a theoretical model based on the imidazolium-functionalised solid **S1**. This study was carried out by using molecular dynamics calculations with force-field methods and clearly shows that the interaction of the imidazolium-functionalised surface with long-chain carboxylate ions significantly decreases the pore size in agreement with the dye delivery inhibition observed experimentally.

Experimental Section

Methods: XRD, TGA, elemental analysis, TEM, nitrogen adsorption/desorption and UV/Vis spectroscopic techniques were employed to characterise the synthesised materials. TGA was carried out on a TGA/SDTA 851e Mettler Toledo balance using an oxidant atmosphere (air; 80 mL min^{-1}) with a heating program that consisted of a ramp of 10 °C min^{-1} from 393 to 1273 K. X-ray measurements were performed on a Bruker AXS D8 Advanced diffractometer using $Cu_{K\alpha}$ radiation. Nitrogen adsorption/desorption isotherms were recorded on a Micromeritics ASAP2010 automated sorption analyser. The samples were degassed at 120 °C in a vacuum overnight. The specific surface area was calculated from the adsorption data in the low-pressure range by using the BET model. The pore size was determined following the BJH method. UV/Vis spectroscopic analysis was carried out with a Lambda 35 UV/Vis spectrometer (Perkin–Elmer Instruments). The UV/Vis spectra of the solids were recorded using a spectrophotometer (Model Perkin–Elmer Lambda) equipped with a diffuse reflectance accessory (Model RSA-PE-20, Labsphere, Inc., North Sutton, NH, USA). The measurements were conducted at room temperature over a wavelength range of $\lambda = 350$–800 nm with a wavelength step of 1 nm. The reflectance data were transformed using the Kubelka–Munk function.[51]

Reagents and solutions: For the synthesis of the mesoporous material, tetraethylorthosilicate (TEOS), *n*-cetyltrimethylammonium bromide (CTAB) and triethanolamine ($TEAH_3$) were obtained from Aldrich. Sodium hydroxide was purchased from Scharlab. For the synthesis of the imidazolium derivative, *N*-methylimidazole was obtained from Acros Organics and 3-(chloropropyl)trimethoxysilane from Fluka. For the preparation of the urea and thiourea derivatives, 3-aminopropyltrimethoxysilane, phenyl isothiocyanate and phenyl isocyanate were obtained from Sigma–Aldrich and were used without any further purification. The dye tris(2,2′-bipyridyl)ruthenium(II) chloride hexahydrate $[Ru(bipy)_3]Cl_2 \cdot 6H_2O$ was purchased from Sigma–Aldrich. All the used sodium carboxylate salts were purchased from Sigma Aldrich.

Synthesis of *N*-methyl-*N*′-propyltrimethoxysilylimidazolium chloride (1): This compound was prepared following a slightly different procedure to that recently reported by Valkenberg et al.[52] A mixture of *N*-methylimidazole (6.57 g, 80 mmol) and 3-(chloropropyl)trimethoxysilane (15.89 g, 80 mmol) were stirred in a dry 100 mL flask under nitrogen flow at 95 °C for 24 h. After cooling at room temperature, the resulting liquid product was extracted with diethyl ether. The final compound was obtained as a yellow liquid.

Synthesis of *N*-phenyl-*N*′-[3-(trimethoxysilyl)propyl]thiourea (2): This product was prepared following a reported procedure[53] by the reaction between 3-(aminopropyl)trimethoxysilane and phenyl isothiocyanate at 50 °C in CH_3Cl (50 mL) in the presence of a few drops of triethylamine.

Synthesis of *N*-phenyl-*N*′-[3-(trimethoxysilyl)propyl]urea (3): This compound was synthesised by the reaction between 3-(aminopropyl)trimethoxysilane (3.49 mL, 20 mmol) and phenyl isocyanate (2.17 mL, 20 mmol) in anhydrous acetonitrile (15 mL) with a few drops of triethylamine as a catalyst. The mixture was stirred in a dry 50 mL flask under argon flow at 80 °C for 15 h. After the mixture had been at room temperature, the solvent was removed by evaporation. The final compound was obtained as a yellow liquid. ^{1}H NMR (300 MHz, $CDCl_3$, 25 °C): $\delta = 0.58$ (t, 2H; CH_2Si), 1.56 (t, 2H; CH_2CH_2Si), 3.16 (t, 2H; $NHCH_2CH_2$), 3.49 (s, 9H; CH_3O), 5.19 (s, 1H; $CONHCH_2$), 6.79 (,1H; C_6H_5NHCS), 6.99 (s, 1H; $CSNHC_6H_5$), 7.22 ppm (m, 4H; C_6H_5NHCS); ^{13}C NMR (75 MHz, $CDCl_3$, 25 °C): $\delta = 7.6$ (CH_2Si), 23.7 (CH_2CH_2Si), 42.1 ($NHCH_2CH_2$), 50.5 (CH_3O), 119.8 (C_6H_5NH), 122.7 (C_6H_5NH), 128.9 (C_6H_5NH), 139.3 (C_6H_5NH), 157.1 ppm (NHCONH); HRMS: *m*/*z*: calcd for $C_{13}H_{22}N_2O_4Si$: 298.1348; found: 298.1357.

MCM-41: The mesoporous MCM-41 support was synthesised by following the so-called "atrane route",[54] a simple preparative technique based on the use of complexes that include $TEAH_3$-related ligands (i.e., in general "atranes" and silatranes for the silicon-containing complexes), TEOS as hydrolytic inorganic precursors and a surfactant as a porogen species. The molar ratio of the reagents in the mother liquor was fixed at

$TEAH_3$/TEOS/CTAB/NaOH/H_2O = 7:2:0.52:0.5:180. In a typical synthesis, $TEAH_3$ (25.79 g, 0.173 mol) and NaOH (0.49 g, 0.012 mol) dissolved in water (2 mL) were stirred, heated to 120 °C and cooled to 70 °C. TEOS (11 mL, 0.049 mol) was added to the reaction mixture and heated to 120 °C to remove the ethanol released during formation of the atrane complexes. CTAB (4.68 g, 0.013 mol) was gradually added. The liquid was cooled to 70 °C and water (80 mL, 4.4 mol) was added with vigorous stirring. After a few minutes, a white suspension was formed. The mixture was subsequently aged at room temperature overnight. The resulting powder was collected by filtration, washed with water and dried at 70 °C, thus producing the as-synthesised MCM-41. The as-synthesised solid was calcined at 550 °C in an oxidant atmosphere for 5 h to remove the template phase, thus yielding the final MCM-41 porous material.

S1: In a typical synthesis, template-free MCM-41 (1.0 g) and the dye tris(2,2′-bipyridyl)ruthenium(II) chloride (0.6 g, 0.8 mmol) were suspended in anhydrous acetonitrile (40 mL) inside a round-bottomed flask connected to a Dean–Stark trap apparatus in an inert atmosphere. The suspension was heated to reflux (120 °C) in an azeotropic distillation and 10 mL of liquid was collected in the trap to remove the adsorbed water. The suspension was stirred for 24 h at room temperature to load the pores of the MCM-41 scaffolding. An excess of *N*-methyl-*N*′-propyltrimethoxysilylimidazolium chloride (2.805 g, 10 mmol) was added to the reaction mixture and the suspension was stirred for 5.5 h. The final orange solid **S1** was removed by filtration, washed with acetonitrile and dried at 70 °C for 12 h.

A similar material was prepared for comparison as a control solid with a fumed-silica support, which lacks the mesoporous structure of the MCM-41-based solids. In a typical synthesis, fumed silica (1.0 g) was suspended in anhydrous acetonitrile (40 mL) inside a round-bottomed flask connected to a Dean–Stark trap apparatus in an inert atmosphere. The suspension was heated to reflux at 120 °C in an azeotropic distillation to remove the adsorbed water. An excess of *N*-methyl-*N*′-propyltrimethoxysilylimidazolium chloride (2.805 g, 10 mmol) was added to the reaction mixture and the suspension was stirred for 5.5 h. The final white solid **FS-Im** was removed by filtration, washed with acetonitrile and dried at 70 °C for 12 h. **FS-Im** consists of a "flat" surface (i.e., without the presence of nanoscopic pores) with anchored imidazolium ions.

S2: In a typical synthesis, template-free MCM-41 (1.00 g) and tris(2,2′-bipyridyl)ruthenium(II) chloride (0.6 g, 0.8 mmol) were suspended in anhydrous acetonitrile (40 mL) inside a round-bottomed flask connected to a Dean–Stark trap apparatus in an inert atmosphere. The suspension was heated to reflux at 120 °C in an azeotropic distillation and 10 mL of liquid was collected in the trap to remove the adsorbed water. The suspension was stirred for 24 h at room temperature to load the pores of the MCM-41 scaffolding. An excess of *N*-phenyl-*N*′-[3-(trimethoxysilyl)propyl]thiourea (3.14 g, 10 mmol) was added to the reaction mixture and the suspension was stirred for 5.5 h. The final orange solid was removed by filtration, washed with acetonitrile and dried at 70 °C for 12 h.

S3: In a typical synthesis, template-free MCM-41 (1.00 g) and tris(2,2′-bipyridyl)ruthenium(II) chloride (0.6 g, 0.8 mmol) were suspended in anhydrous acetonitrile (40 mL) inside a round-bottomed flask connected to a Dean–Stark trap apparatus in an inert atmosphere. The suspension was heated to reflux at 120 °C in an azeotropic distillation and 10 mL of liquid was collected in the trap to remove the adsorbed water. The suspension was stirred for 24 h at room temperature to load the pores of the MCM-41 scaffolding. An excess of *N*-phenyl-*N*′-[3-(trimethoxysilyl)propylurea (2.66 g, 10 mmol) was added to the reaction mixture and the suspension was stirred for 5.5 h. The final orange solid **S3** was removed by filtration, washed with acetonitrile and dried at 70 °C for 12 h.

Dye release studies: Carboxylate recognition studies were carried out using the solid (**S1**–**S3** and **FS-Im**; 10 mg) suspended in aqueous solution (25 mL; buffered at pH 7.0 with HEPES, 10^{-3} mol dm^{-3}) that contained the corresponding carboxylate ion ($c_{carboxylate} = 10^{-3}$ mol dm^{-3}). The suspension was stirred for some minutes to allow maximum dye delivery and removed by filtration with a teflon filter. The release of the $[Ru(bipy)_3]^{2+}$ dye from the pore voids to the aqueous solution was monitored through the spin-allowed metal-to-ligand charge-transfer (MLCT) transition band of the $[Ru(bipy)_3]^{2+}$ dye centred at $\lambda_{max} = 454$ nm.

Computational details

Three requirements must be accomplished by the silica crystal structure chosen to build a suitable two-dimensional model of a mesoporous silica material of the MCM-41 family: 1) one of the surfaces must only present terminal oxygen atoms; 2) the opposite surface should only show terminal silicon atoms that will act as anchoring points for the imidazolium; 3) the morphology of the mesopore must be close to a cylindrical ideal geometry. By attending these conditions, we selected the crystal structure of β-cristobalite. A cleavage of the crystal structure parallel to the (1 −1 1) plane allowed us to obtain a mesoporous model with large quasi-cylindrical nanopores. This model can be described as a hexagonal supercell with the following parameters, $a = b = 40.503$ Å, $\alpha = \beta = 90.0°$ and $\gamma = 120.0°$. The size of this "supercell" was chosen to generate pores and walls with similar dimensions (diameter (d): 22.9 Å, thickness (t): 15.5 Å, respectively) to those experimentally found in MCM-41 family of solids ($d = 23.3$, $t = 13.1$ Å). The deepness of the pores in this two-dimensional model is 28.7 Å. The terminal oxygen atoms in the surfaces and inside the nanopore were protonated. In our system, imidazolium-substituted alkyl ions are anchored in the surface and its chemical function must be to interact with carboxylate ions to limit the free motion of the last molecules that will be in charge of the closing of the pore. Therefore, we labelled the imidazolium substituents as receiver groups. These receiver groups were anchored on the mesoporous surface modelled with the Cerius2 package.[55] All the possible anchoring positions were not used to avoid problems caused by steric effects between neighbouring receivers. On this model, which was considered by us to be a multi-receiver cell (MRC), different carboxylate ions were added to study the mechanism that tunes the closing of the nanopore.

Due to the huge size of the models needed for this kind of study, the calculations were carried out by using force-field methods. For this purpose, the universal force field (UFF) suggested by Rappe et al. was employed.[56] To find the global energy minimum and because of the presence of many local minima, molecular dynamics simulations were carried out to cover the more important parts of the potential-energy surface by using thermal energy to escape from the local minima. These molecular dynamics simulations were carried out within the canonical ensemble (number of particles, volume and temperature were maintained at a constant) for 10 ps with a time step of 1 fs. Among the conformations observed during the molecular dynamics simulation, the most stable geometry was taken as starting point for a later geometry optimisation. The geometry optimisations and molecular dynamics simulations were performed with the Cerius2 package.[55] In the evaluation of the nanopore diameter, the Van der Waals radii provided by the Cerius2 package for each element were used. In fact, this parameter represents the maximum diameter of a sphere that moves freely into and out of the nanopore.

DFT calculations were carried out on the singlet spin states of the imidazolium-substituted alkyl molecule with the hybrid B3LYP method,[57] as implemented in the Gaussian 03 program,[58] with the triple-ζ quality basis sets proposed by Ahlrichs and co-workers.[59] The electronic-density data were obtained from NBO analysis.[60]

Acknowledgements

We thank the Spanish Ministerio de Educación y Ciencia (Project CTQ2006-15456-C04-01/BQU) and the Generalitat Valenciana (Project GV06/101) for their support. C.C. is grateful to the Universidad Politécnica de Valencia for the award of a doctoral fellowship. E.A. thanks the Ministerio de Ciencia e Inovación for an FPU fellowship. We are obliged to the Servicio de Microscopía de la UPV for the use of their TEM facilities.

[1] a) A. B. Descalzo, R. Martínez-Máñez, F. Sancenón, K. Hoffmann, K. Rurack, *Angew. Chem.* **2006**, *118*, 6068–6093; *Angew. Chem. Int. Ed.* **2006**, *45*, 5924–5948; b) K. Ariga, A. Vinu, J. P. Hill, T. Mori,

Coord. Chem. Rev. **2007**, *251*, 2562–2591; c) R. Mártinez-Máñez, F. Sancenón, *Coord. Chem. Rev.* **2006**, *250*, 3081–3093; d) K. Ariga, J. P. Hill, M. V. Lee, A. Vinu, R. Charvet, S. Acharya, *Sci. Technol. Adv. Mater.* **2008**, *9*, 0104109.

[2] M. Hamidi, A. Azadi, P. Rafiei, *Adv. Drug Delivery Rev.* **2008**, *60*, 1638–1649.

[3] C. W. Pouton, C. J. H. Porter, *Adv. Drug Delivery Rev.* **2008**, *60*, 625–637.

[4] C. J. F. Rijcken, O. Soga, W. E. Hennink, C. F. van Nostrum, *J. Controlled Release* **2007**, *120*, 131–148.

[5] a) C. T. Kresge, M. E. Leonowicz, W. J. Roth, J. C. Vartuli, J. S. Beck, *Nature* **1992**, *359*, 710–711; b) F. Hoffmann, M. Cornelius, M. Morell, M. Fröba, *Angew. Chem.* **2006**, *118*, 3290–3328; *Angew. Chem. Int. Ed.* **2006**, *45*, 3216–3251.

[6] a) N. K. Mal, M. Fujiwara, Y. Tanaka, *Nature* **2003**, *421*, 350–353; b) N. K. Mal, M. Fujiwara, Y. Tanaka, T. Taguchi, M. Matsukata, *Chem. Mater.* **2003**, *15*, 3385–3394.

[7] Y. Zhu, M. Fujiwara, *Angew. Chem.* **2007**, *119*, 2291–2294; *Angew. Chem. Int. Ed.* **2007**, *46*, 2241–2244.

[8] a) J. Lu, E. Choi, F. Tamanoi, J. I. Zink, *Small* **2008**, *4*, 421–426; b) S. Angelos, E. Vhoi, F. Vögtle, L. De Cola, J. I. Zink, *J. Phys. Chem. C* **2007**, *111*, 6589–6592.

[9] N. Liu, D. Dunphy, P. Atanassov, S. D. Bunge, Z, Chen, G. P. López, T. J. Boyle, C. J. Brinker, *Nano Lett.* **2004**, *4*, 551–554.

[10] D. P. Ferris, Y. L. Zhao, N. M. Khashab, H. A. Khatib, J. F. Stoddart, J. I. Zink, *J. Am. Chem. Soc.* **2009**, *131*, 1686–1688.

[11] E. Aznar, R. Casasús, B. García-Acosta, M. D. Marcos, R. Martínez-Máñez, F. Sancenón, J. Soto, P. Amorós, *Adv. Mater.* **2007**, *19*, 2228–2231.

[12] a) R. Casasús, M. D. Marcos, R. Martínez-Máñez, J. V. Ros-Lis, J. Soto, L. A. Villaescusa, P. Amorós, D. Beltrán, C. Guillem, J. Latorre, *J. Am. Chem. Soc.* **2004**, *126*, 8612–8613; b) R. Casasús, E. Climent, M. D. Marcos, R. Martínez-Máñez, F. Sancenón, J. Soto, P. Amorós, J. Cano, E. Ruiz, *J. Am. Chem. Soc.* **2008**, *130*, 1903–1917.

[13] A. Bernardos, E. Aznar, C. Coll, R. Martínez-Máñez, J. M. Barat, M. D. Marcos, F. Sancenón, J. Soto, *J. Controlled Release* **2008**, *131*, 181–189.

[14] Q. Yang, S. Wang, P. Fan, L. Wang, Y. Di, K. Lin, F. S. Xiao, *Chem. Mater.* **2005**, *17*, 5999–6003.

[15] T. D. Nguyen, K. C. F. Leung, M. Liong, C. D. Pentecost, J. F. Stoddart, J. I. Zink, *Org. Lett.* **2006**, *8*, 3363–3366.

[16] K. C. F. Leung, T. D. Nguyen, J. F. Stoddart, J. I. Zink, *Chem. Mater.* **2006**, *18*, 5919–5928.

[17] S. Angelos, Y. W. Yang, K. Patel, J. F. Stoddart, J. I. Zink, *Angew. Chem.* **2008**, *120*, 2254–2258; *Angew. Chem. Int. Ed.* **2008**, *47*, 2222–2226.

[18] N. M. Khashab, A. Trabolsi, Y. A. Lau, M. W. Ambrogio, D. C. Friedman, H. A. Khatib, J. I. Zink, J. F. Stoddart, *Eur. J. Org. Chem.* **2009**, 1669–1673.

[19] C. Park, K. Oh, S. C. Lee, C. Kim, *Angew. Chem.* **2007**, *119*, 1477–1479; *Angew. Chem. Int. Ed.* **2007**, *46*, 1455–1457.

[20] E. Aznar, M. D. Marcos, R. Martínez-Máñez, F. Sancenón, J. Soto, P. Amorós, C. Guillem, *J. Am. Chem. Soc.* **2009**, *131*, 6833–6843.

[21] a) B. G. Trewyn, S. Giri, I. I. Slowing, V. S. Y. Lin, *Chem. Commun.* **2007**, 3236–3245; b) B. G. Trewyn, I. I. Slowing, S. Giri, H. T. Chen, V. S. Y. Lin, *Acc. Chem. Res.* **2007**, *40*, 846–853; c) C. Y. Lai, B. G. Trewyn, D. M. Jeftinija, K. Jeftinija, S. Xu, S. Jeftinija, V. S. Y. Lin, *J. Am. Chem. Soc.* **2003**, *125*, 4451–4459; d) F. Torney, B. G. Trewyn, V. S. Y. Lin, K. Wang, *Nat. Nanotechnol.* **2007**, *2*, 295–300; e) D. R. Radu, C. Y. Lai, K. Jeftinija, E. W. Rowe, S. Jeftinija, V. S.-Y. Lin, *J. Am. Chem. Soc.* **2004**, *126*, 13216–13217; f) S. Giri, B. G. Trewyn, M. P. Stellmaker, V. S.-Y. Lin, *Angew. Chem.* **2005**, *117*, 5166–5172; *Angew. Chem. Int. Ed.* **2005**, *44*, 5038–5044; g) I. I. Slowing, B. G. Trewyn, V. S.-Y. Lin, *J. Am. Chem. Soc.* **2007**, *129*, 8845–8849; h) I. I. Slowing, B. G. Trewyn, S. Giri, V. S.-Y. Lin, *Adv. Funct. Mater.* **2007**, *17*, 1225–1236; i) J. L. Vivero-Escoto, I. I. Slowing, C. Y. Wu, V. S. Y. Lin, *J. Am. Chem. Soc.* **2009**, *131*, 3462–3463; j) R. Mortera, J. Vivero-Escoto, I. I. Slowing, E. Garrone, B. Onida, V. S. Y. Lin, *Chem. Commun.* **2009**, 3219–3221; k) Y. Zhao, B. G. Trewyn, I. I. Slowing, V. S. Y. Lin, *J. Am. Chem. Soc.* **2009**, *131*, 8398–8400.

[22] R. Hernandez, H. R. Tseng, J. W. Wong, J. F. Stoddart, J. I. Zink, *J. Am. Chem. Soc.* **2004**, *126*, 3370–3371.

[23] T. D. Nguyen, H. R. Tseng, P. C. Celeste, A. H. Flood, Y. Liu, J. F. Stoddart, J. I. Zink, *Proc. Natl. Acad. Sci. USA* **2005**, *102*, 10029–10034.

[24] T. D. Nguyen, Y. Liu, S. Saha, K. C. F. Leung, J. F. Stoddart, J. I. Zink, *J. Am. Chem. Soc.* **2007**, *129*, 626–634.

[25] T. D. Nguyen, K. C. F. Leung, M. Liong, Y. Liu, J. F. Stoddart, J. I. Zink, *Adv. Funct. Mater.* **2007**, *17*, 2101–2110.

[26] M. Fujiwara, S. Terashima, Y. Endo, K. Shiokawa, H. Ohue, *Chem. Commun.* **2006**, 4635–4637.

[27] R. Liu, X. Zhao, T. Wu, P. Feng, *J. Am. Chem. Soc.* **2008**, *130*, 14418–14419.

[28] Q. Fu, G. V. R. Rao, L. K. Ista, Y. Wu, B. P. Andrzejewski, L. A. Sklar, T. L. Ward, G. P. López, *Adv. Mater.* **2003**, *15*, 1262–1266.

[29] K. Patel, S. Angelos, W. R. Dichtel, A. Coskun, Y. W. Yang, J. I. Zink, J. F. Stoddart, *J. Am. Chem. Soc.* **2008**, *130*, 2382–2383.

[30] A. Schlossbauer, J. Kecht, T. Bein, *Angew. Chem.* **2009**, *121*, 3138–3141; *Angew. Chem. Int. Ed.* **2009**, *48*, 3092–3095.

[31] A. Bernardos, E. Aznar, M. D. Marcos, R. Martínez-Máñez, F. Sancenón, J. Soto, J. M. Barat, P. Amorós, *Angew. Chem.* **2009**, *121*, 5998–6001; *Angew. Chem. Int. Ed.* **2009**, *48*, 5884–5887.

[32] E. Climent, A. Bernardos, R. Martínez-Máñez, A. Maquieira, M. D. Marcos, N. Pastor-Navarro, R. Puchades, F. Sancenón, J. Soto, P. Amorós, *J. Am. Chem. Soc.* **2009**, *131*, 14075–14080.

[33] R. Casasús, E. Aznar, M. D. Marcos, R. Martínez-Máñez, F. Sancenón, J. Soto, P. Amorós, *Angew. Chem.* **2006**, *118*, 6813–6816; *Angew. Chem. Int. Ed.* **2006**, *45*, 6661–6664.

[34] E. Aznar, C. Coll, M. D. Marcos, R. Martínez-Máñez, F. Sancenón, J. Soto, P. Amorós, J. Cano, E. Ruíz, *Chem. Eur. J.* **2009**, *15*, 6877–6888.

[35] E. Climent, M. Dolores Marcos, R. Martínez-Máñez, F. Sancenón, J. Soto, K. Rurack, P. Amorós, *Angew. Chem.* **2009**, *121*, 8671–8674; *Angew. Chem. Int. Ed.* **2009**, *48*, 8519–8522.

[36] C. Coll, R. Casasús, E. Aznar, M. D. Marcos, R. Martínez-Máñez, F. Sancenón, J. Soto, P. Amorós, *Chem. Commun.* **2007**, 1957–1959.

[37] See, for example: a) J. Y. Kwon, N. J. Singh, H. Kim, S. K. Kim, K. S. Kim, J. Yoon, *J. Am. Chem. Soc.* **2004**, *126*, 8892–8893; b) S. K. Kim, B.-G. Kang, H. S. Koh, Y. J. Yoon, S. J. Jung, B. Jeong, K.-D. Lee, J. Yoon, *Org. Lett.* **2004**, *6*, 4655–4658; c) J. Yoon, S. K. Kim, N. J. Singh, J. W. Lee, Y. J. Yang, K. Chellappan, K. S. Kim, *J. Org. Chem.* **2004**, *69*, 581–583; d) C. E. Willans, K. M. Anderson, P. C. Junk, L. J. Barbour, J. W. Steed, *Chem. Commun.* **2007**, 3634–3636; e) J. Yoon, S. K. Kim, N. J. Singh, K. S. Kim, *Chem. Soc. Rev.* **2006**, *35*, 355–360.

[38] See, for example: a) V. Amendola, D. Estebán-Gómez, L. Fabbrizzi, M. Licchelli, *Acc. Chem. Res.* **2006**, *39*, 343–353; b) M. Boiocchi, L. Del Boca, D. Estebán-Gómez, L. Fabbrizzi, M. Licchelli, E. Monzani, *Chem. Eur. J.* **2005**, *11*, 3097–3104; c) J. Y. Kwon, Y. J. Jang, S. K. Kim, K. H. Lee, J. S. Kim, J. Yoon, *J. Org. Chem.* **2004**, *69*, 5155–5157; d) E. Quinlan, S. E. Matthews, T. Gunnlaugsson, *J. Org. Chem.* **2007**, *72*, 7497–7503; e) C. M. G. dos Santos, T. McCabe, G. W. Watson, P. E. Kruger, T. Gunnlaugsson, *J. Org. Chem.* **2008**, *73*, 9235–9244; f) D. A. Jose, D. K. Kumar, B. Ganguly, A. Das, *Org. Lett.* **2004**, *6*, 3445–3448.

[39] S. Brunauer, P. H. Emmet, E. Teller, *J. Am. Chem. Soc.* **1938**, *60*, 309–319.

[40] E. P. Barrett, L. G. Joyner, P. P. Haselda, *J. Am. Chem. Soc.* **1951**, *73*, 373–380.

[41] See, for example in *Tietz Fundamentals of Clinical Chemistry*, 4th ed. (Eds.: C. A. Burtis, E. R. Ashwood), Saunders, Philadelphia, **1995**, pp. 338–442.

[42] J. Jackson, *A User's Guide to Principal Components*, Wiley, New York, **1991**.

[43] a) A. M. Costero, S. Peransi, S. Gil, *Tetrahedron Lett.* **2006**, *47*, 6561–6564; b) T. D. Thangadurai, N. J. Singh, I. C. Hwang, J. W. Lee, R. P. Chandran, K. S. Kim, *J. Org. Chem.* **2007**, *72*, 5461–5464;

c) Y. P. Tseng, G. M. Tu, C. H. Lin, C. T. Chang, C. Y. Lin, Y. P. Yen, *Org. Biomol. Chem.* **2007**, *5*, 3592–3598.

[44] a) A. Metzger, E. V. Anslyn, *Angew. Chem.* **1998**, *110*, 682–684; *Angew. Chem. Int. Ed.* **1998**, *37*, 649–652; b) S. L. Wiskur, E. V. Anslyn, *J. Am. Chem. Soc.* **2001**, *123*, 10109–10110; c) J. J. Lavigne, E. V. Anslyn, *Angew. Chem.* **1999**, *111*, 3903–3906; *Angew. Chem. Int. Ed.* **1999**, *38*, 3666–3669; d) F. Sancenón, R. Martínez-Máñez, M. A. Miranda, M. J. Seguí, J. Soto, *Angew. Chem.* **2003**, *115*, 671–674; *Angew. Chem. Int. Ed.* **2003**, *42*, 647–650; e) M. Boiocchi, M. Bonizzoni, L. Fabbrizzi, G. Piovani, A. Taglietti, *Angew. Chem.* **2004**, *116*, 3935–3940; *Angew. Chem. Int. Ed.* **2004**, *43*, 3847–3852.

[45] C. Coll, R. Martínez-Máñez, M. D. Marcos, F. Sancenón, J. Soto, *Angew. Chem.* **2007**, *119*, 1705–1708; *Angew. Chem. Int. Ed.* **2007**, *46*, 1675–1678.

[46] See, for example: a) S. Alegret, J. Alonso, J. Bartroli, J. Baro-Roma, J. Sanchez, M. del Valle, *Analyst* **1994**, *119*, 2319–2322; b) K. Vytras, J. Kalous, J. Jezkova, *Egypt. J. Anal. Chem.* **1997**, *6*, 107–123; c) R. Schulz, P. Bruttel, H. Reger, G. Wulk, J. Thiede, R. Unthan, C. Götz in *Titrimetric Determination of Surfactants and Pharmaceuticals*, METROHM, Switzerland, **1999**, p. 242.

[47] See, for example: a) T. Saito, K. Higashi, G. Hagiwara, *Fresenius J. Anal. Chem.* **1982**, *313*, 21–23; b) M. Y. Ye, R. G. Walkup, K. D. Hill, *J. Liq. Chromatogr.* **1994**, *17*, 4087–4097.

[48] See, for example: a) F. Canete, A. Rios, M. D. Luque de Castro, M. Valcarcel, *Anal. Chem.* **1988**, *60*, 2354–2357; b) H. Liu, P. K. Dasgupta, *Anal. Chim. Acta* **1994**, *288*, 237–245; c) S. Motomizu, Y. H. Gao, K. Uemura, S. Ihsibara, *Analyst* **1994**, *119*, 473–477.

[49] See, for example: a) S. Rubio-Barroso, M. Gómez-Rodríguez, L. M. Polo-Diez, *Microchem. J.* **1988**, *37*, 93–98; b) S. Rubio-Barroso, V. Rodríguez-Gamonal, L. M. Polo-Diez, *Anal. Chim. Acta* **1988**, *206*, 351–355.

[50] a) F. A. Chmilenko, I. V. Koroboca, L. N. Danilenko, *J. Anal. Chem.* **2000**, *50*, 1058–1062; b) J. Sánchez, M. del Valle, *Talanta* **2001**, *54*, 893–902; c) B. Kovács, B. Csóka, G. Nagy, A. Ivaska, *Anal. Chim. Acta* **2001**, *437*, 67–76; d) S. Matysik, F. M. Matysik, W. D. Einicke, *Sens. Actuators B* **2002**, *85*, 104–108; e) H. Fukui, A. Kaminaga, T. Maeda, K. Hayakawa, *Anal. Chim. Acta* **2003**, *481*, 221–228; f) M. Arvand-Barmchi, M. F. Mousavi, M. A. Zanjanchi, M. Shamsipur, *Microchem. J.* **2003**, *74*, 149–156; g) M. J. Seguí, J. Lizondo-Sabater, A. Benito, R. Martínez-Máñez, T. Pardo, F. Sancenón, J. Soto, *Talanta* **2007**, *71*, 333–338; h) M. J. Seguí, J. Lizondo-Sabater, R. Martínez-Máñez, T. Pardo, F. Sancenón, J. Soto, *Anal. Chim. Acta* **2004**, *525*, 83–90.

[51] A. V. Zinchuk, B. C. Hancock, E. Y. Shalaev, R. D. Reddy, R. Govindarajan, E. Novak, *Eur. J. Pharm. Biopharm.* **2005**, *61*, 158–170.

[52] M. H. Valkenberg, C. de Castro, W. F. Hölderich, *Top. Catal.* **2000**, *14*, 139–144.

[53] P. Calero, R. Martínez-Máñez, F. Sancenón, J. Soto, *Eur. J. Inorg. Chem.* **2008**, 5649–5658.

[54] S. Cabrera, J. El Haskouri, C. Guillem, J. Latorre, A. Beltrán, D. Beltrán, M. D. Marcos, P. Amorós, *Solid State Sci.* **2000**, *2*, 405–420.

[55] Cerius2, version 3.8, Molecular Simulations Inc., San Diego, **1998**.

[56] a) A. K. Rappe, C. J. Casewith, K. S. Colwell, W. A. Goddard III, W. M. Skiff, *J. Am. Chem. Soc.* **1992**, *114*, 10024–10035; b) L. A. Castonguay, A. K. Rappe, *J. Am. Chem. Soc.* **1992**, *114*, 5832–5842; c) A. K. Rappe, K. S. Colwell, *Inorg. Chem.* **1993**, *32*, 3438–3450.

[57] a) A. D. Becke, *Phys. Rev. A* **1988**, *38*, 3098–3100; b) C. T. Lee, W. T. Yang, R. G. Parr, *Phys. Rev. B* **1988**, *37*, 785–789; c) A. D. Becke, *J. Chem. Phys.* **1993**, *98*, 5648–5652.

[58] Gaussian 03, Revision C.02, M. J. Frisch, G. W. Trucks, H. B. Schlegel, G. E. Scuseria, M. A. Robb, J. R. Cheeseman, J. A. Montgomery, Jr., T. Vreven, K. N. Kudin, J. C. Burant, J. M. Millam, S. S. Iyengar, J. Tomasi, V. Barone, B. Mennucci, M. Cossi, G. Scalmani, N. Rega, G. A. Petersson, H. Nakatsuji, M. Hada, M. Ehara, K. Toyota, R. Fukuda, J. Hasegawa, M. Ishida, T. Nakajima, Y. Honda, O. Kitao, H. Nakai, M. Klene, X. Li, J. E. Knox, H. P. Hratchian, J. B. Cross, V. Bakken, C. Adamo, J. Jaramillo, R. Gomperts, R. E. Stratmann, O. Yazyev, A. J. Austin, R. Cammi, C. Pomelli, J. W. Ochterski, P. Y. Ayala, K. Morokuma, G. A. Voth, P. Salvador, J. J. Dannenberg, V. G. Zakrzewski, S. Dapprich, A. D. Daniels, M. C. Strain, O. Farkas, D. K. Malick, A. D. Rabuck, K. Raghavachari, J. B. Foresman, J. V. Ortiz, Q. Cui, A. G. Baboul, S. Clifford, J. Cioslowski, B. B. Stefanov, G. Liu, A. Liashenko, P. Piskorz, I. Komaromi, R. L. Martin, D. J. Fox, T. Keith, M. A. Al-Laham, C. Y. Peng, A. Nanayakkara, M. Challacombe, P. M. W. Gill, B. Johnson, W. Chen, M. W. Wong, C. Gonzalez, J. A. Pople, Gaussian, Inc., Wallingford CT, **2004**.

[59] a) A. Schäfer, H. Horn, R. Ahlrichs, *J. Chem. Phys.* **1992**, *97*, 2571–2577; b) A. Schäfer, C. Huber, R. Ahlrichs, *J. Chem. Phys.* **1994**, *100*, 5829–5838.

[60] a) F. Weinhold, J. E. Carpenter, *J. Mol. Struct.* **1988**, *172–191*, 189–202; b) A. E. Reed, L. A. Curtiss, F. Weinhold, *Chem. Rev.* **1988**, *88*, 899–926; c) F. Weinhold, J. E. Carpenter in *The Structure of Small Molecules and Ions*, Plenum Press, New York, **1988**, p. 227.

Received: November 13, 2009
Revised: April 23, 2010
Published online: July 19, 2010

